ACOUSTIC EMISSION MONITORING OF A

GROUND DURABILITY AND DAMAGE TOLERANCE TEST

Stuart McBride, Melvyn Viner, and Michael Pollard
Department of Physics
Royal Military College of Canada
Kingston, ON   K7K 5L0

INTRODUCTION

Since the mid-1970's several authors have investigated the feasibility of using acoustic emission to monitor the integrity of aircraft structures. These studies, which have involved the monitoring of airframes during full scale ground fatigue tests as well as the monitoring of airframe components during flight, are completely catalogued in Drouillard's annotated bibliography of acoustic emission [1,2]. In the future, acoustic emission is expected to play a primary role in the evaluation of the structural integrity of complex bolted structures such as airframes because of its ability to monitor large areas using a relatively small number of sensors. This work demonstrates the successful application to such a problem involving the monitoring of the lower wing skin of a fighter aircraft. The monitored area contained approximately 600 fasteners which attach the lower wing skin to the inner structure.

EXPERIMENTAL

The Data Acquisition System

The 16 channel instrumentation system is based on the dual-channel acoustic emission system developed at the Royal Military College of Canada. This data acquisition system (commercially available from AEMS, Acoustic Emission Monitoring Services Inc., Kingston, Ontario, Canada) was designed and constructed specifically for the recording and interpreting of acoustic emission data in the laboratory and during flight. The design is based on criteria derived from the RMC work of almost a decade in the area of acoustic emission monitoring during flight [3,4,5,6]. These studies established the importance of the difference in arrival time of an event at different locations, signal risetime, and the magnitude and variation of the applied stress at the time of occurrence of the event. All of these parameters are necessary to isolate crack-related events from other noise sources during dynamic loading of a large, dispersive structure and are recorded by the data acquisition system used here. To provide maximum flexibility, the data acquisition system is designed to use either an available 115/230V, 47-440Hz electrical supply or internal batteries.

The output of each piezoelectric sensor element is amplified by a preamplifier with nominal gain of 40 dB. The resulting signal is buffered, logarithmically amplified, envelope followed and peak detected. These operations are accomplished using signal conditioning modules custom-made for the purpose (Figure 1a). The output of each envelope follower is separately fed into the digital data acquisition system which records the times of pre-selected amplitude threshold crossings 6 dB apart (Figure 1b). The output of the peak detectors and strain gauge are digitized and stored in memory.
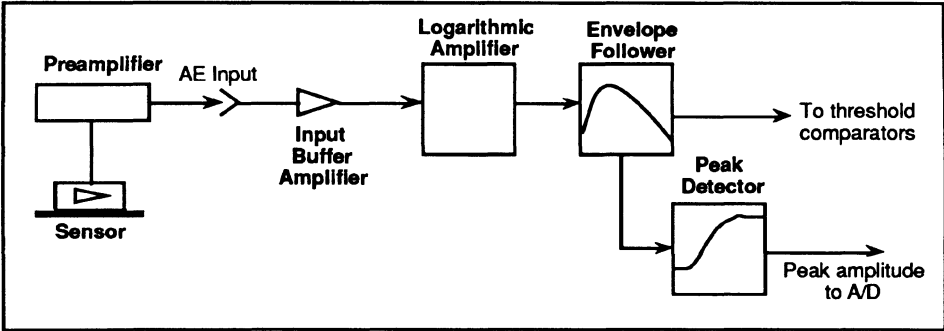
Fig. 1b. Schematic diagram of the AEMS acoustic emission data acquisition computer.
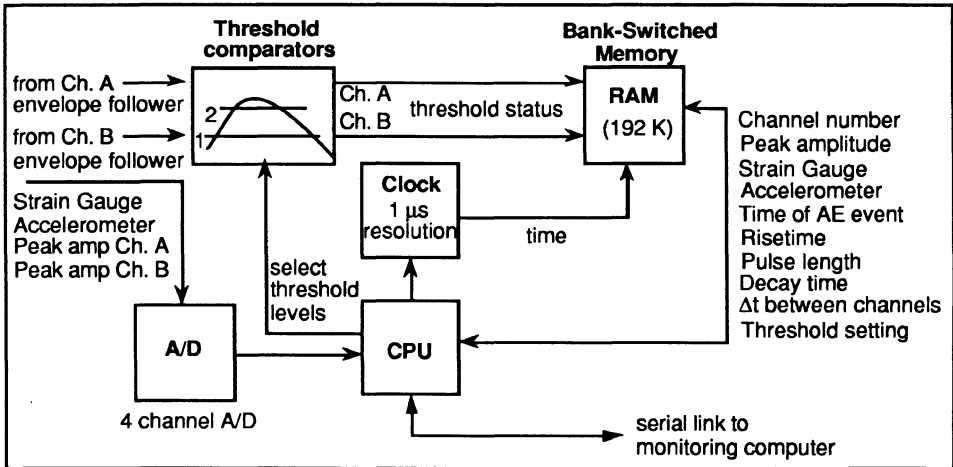

Fig. 1a. Schematic diagram of the AEMS acoustic emission signal conditioning.

All of the above data are compressed into an event record which includes the time of occurrence of the event at each sensor, the difference in arrival times at two sensors (Δt), event risetimes for 6 dB change in amplitude, event durations, event decay times and event peak amplitudes. The resulting data set is then extracted from the data acquisition system via an RS-232 interface and stored on disk on an external portable computer. By using a data multiplexer, several 2-channel systems are operated in parallel to achieve multi-channel capability. Since each 2-channel system has a CPU there is no decrease in data acquisition rate as the number of channels is increased. Extensive screening of data, field analysis and interpretation can be carried out immediately on the host monitoring computer. Final analysis and interpretation are accomplished using spreadsheet software. Table 1 lists the general specifications of the apparatus.

Monitored Regions

The regions monitored were selected by the fatigue test engineers and are located on the lower wing skin of a fighter aircraft. The particular areas of interest are the 15% spar regions between the indicated sensor locations and the 39% and 44% spar regions within the linear array of sensors as shown in Figure 2. The precise location of each sensor is constrained by the presence of the pads which are used to transmit the simulated flight loads to the wing.

Table 1. General specifications for the AEMS digital data acquisition system for in-flight acoustic emission monitoring applications.

2 Channels AE	60 dB dynamic range
2 Analog Channels	10 V full-scale
Power Supply	115/230V, 47-440 Hz or battery powered
Power Consumption	10 Watts maximum
Data Storage Capacity	192 or 384 Kbyte RAM with battery back-up
Dimensions	23 cm x 13.5 cm x 25 cm
Weight	2 kg
Mass Data Storage	RS232 transfer to external computer
Windowing on all recorded parameters	Available on-line and during post analysis

Wing Loading

Fatigue cycling loads were applied at various loading points to simulate the known flight load spectra measured on flying aircraft. The actual loadings used are defined in terms of the in-flight acceleration of the aircraft (g) or the corresponding transverse strain measured by strain gauges attached to the lower wing skin. Table 2 lists the simulated flight load spectrum in terms of g and the normalized percent transverse strain relative to the value at 7g measured on the lower wing skin. The output of the strain gauge is recorded by the data acquisition system as the measure of the wing loading conditions at the time of occurrence of each acoustic emission signal. The highest strain maneuvers (6.5g and 7g) are of particular interest for the acoustic emission monitoring since they provide the highest loads, and hence, the most probable circumstances for crack advance acoustic emissions.

Acoustic Emission System Calibration

Pencil lead fracture was used to obtain the area calibration of the various acoustic emission parameters (Δt, pulse length, risetime, etc). It was found that, close to the array, the difference in arrival time at neighboring sensors is linear and results from an acoustic wave velocity of 2km/s. The measured risetime of the signals detected by the Dunegan Endevco D9202A sensors was less than 3µs and was essentially independent of source position between the sensors provided no abrupt changes in material thickness occurred. Such changes in the thickness usually involved additional fasteners to connect the wing skin to the substructure, and hence, introduced additional reflections. The amplitude of the detected signal could be reduced by as much as 20dB as a result of such acoustic scattering.
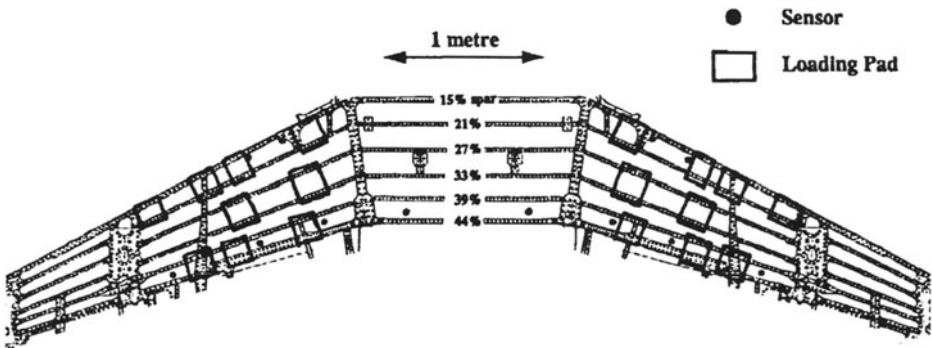

Fig. 2. Schematic diagram of the aircraft lower wing skin showing the location of the acoustic emission sensors and the loading pads in the region of interest.

Table 2. Number of occurrences of maximum g levels per thousand flying hours derived from measurements during typical flight conditions. Also shown is the % strain in the lower wing skin relative to the value at 7g.

g	Strain %	Loadings/10^3 Flying Hrs
4.5	64.3	1770
5.0	71.4	2828
5.5	78.6	1589
6.0	85.7	198
6.5	92.9	45
7.0	100.0	90

The Acoustic Emission Measurements

Initial monitoring was carried out in the forward wing area (15% spar) between the indicated sensor pairs (Figure 2). These regions are known to be prone to fatigue cracking. Acoustic emission data for relative strains greater than 80% (see Table 2) was continuously recorded during dynamic loading. At intervals, a static loading was performed. Figure 3 shows a comparison of the occurrence of acoustic emission events during such static loadings. The data from a cracked location included events occurring during the hold time at maximum loading while those from an uncracked location did not. This behavior is consistent for both static and dynamic loading observations.

Acoustic emission predicted cracks in the regions between each of the sensor pairs at the 15% spar. Each of these defects was located by acoustic emission via difference in arrival time for each pair of sensors together with risetime gating of signals occurring near 100% relative strain (see Table 2). The result obtained from the static tests was in agreement with the predictions of the emissions detected during dynamic loading. Cracks were found in the wing skin at two bolt holes between the sensor pair and in the inner wing structure on the port side. These were confirmed using eddy current and liquid penetrant inspection. Similarly, on the starboard side, between the sensor pair, one crack was found and confirmed at a bolt hole in the wing skin and also in the inner wing structure. The damage just described was repaired before proceeding with the fatigue test.
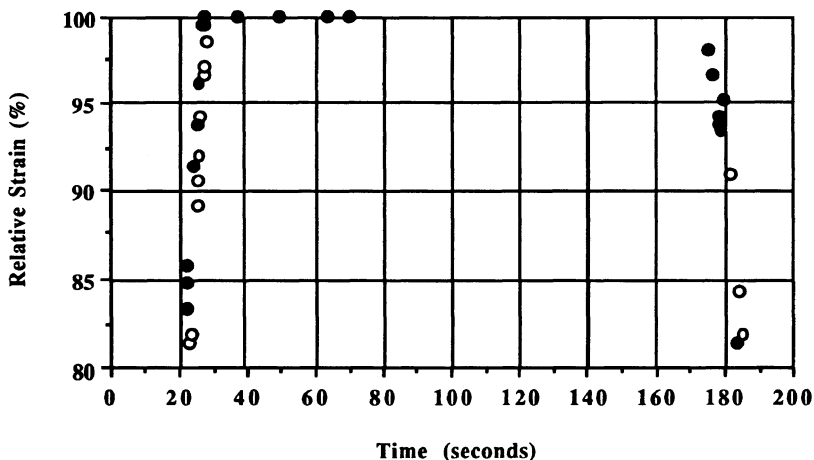

Fig. 3. Acoustic emissions detected from cracked (•) and uncracked (o) locations during a static loading test. Note the presence of emissions during the hold time at maximum loading for the cracked location only.

During the inspection described above (which resulted in repair of the 15% spar) damage was detected by NDT (eddy current and liquid penetrant) at fastener holes on the port side of the 44% spar. No damage was found using NDT for the starboard side of the 44% spar. With the sensors positioned between the 39% and 44% spars in the linear array shown in Figure 2, it was shown by monitoring a static loading to 100% relative strain that the 44% spar defects on the port side could be detected and located by acoustic emission. During this static test defects were clearly detected in the starboard side at 1m from the wing centre line but could not be confirmed by NDT inspection. The port side damage in the 44% spar region was repaired and the dynamic loading test continued. The subsequent acoustic emission behaviour during dynamic loading recorded near maximum load (7g, 100% relative strain maneuvers) is shown in Figure 4 indicating substantial activity on the starboard side in the vicinity of 1m from the wing center. For this location emissions near maximum load were detected during the majority of 7g loadings. Such a behavior is consistent with fatigue crack growth. Based on this result, dynamic loading was terminated and a more thorough NDT inspection carried out. Figure 4 compares the results of these NDT inspections with the acoustic emission data.
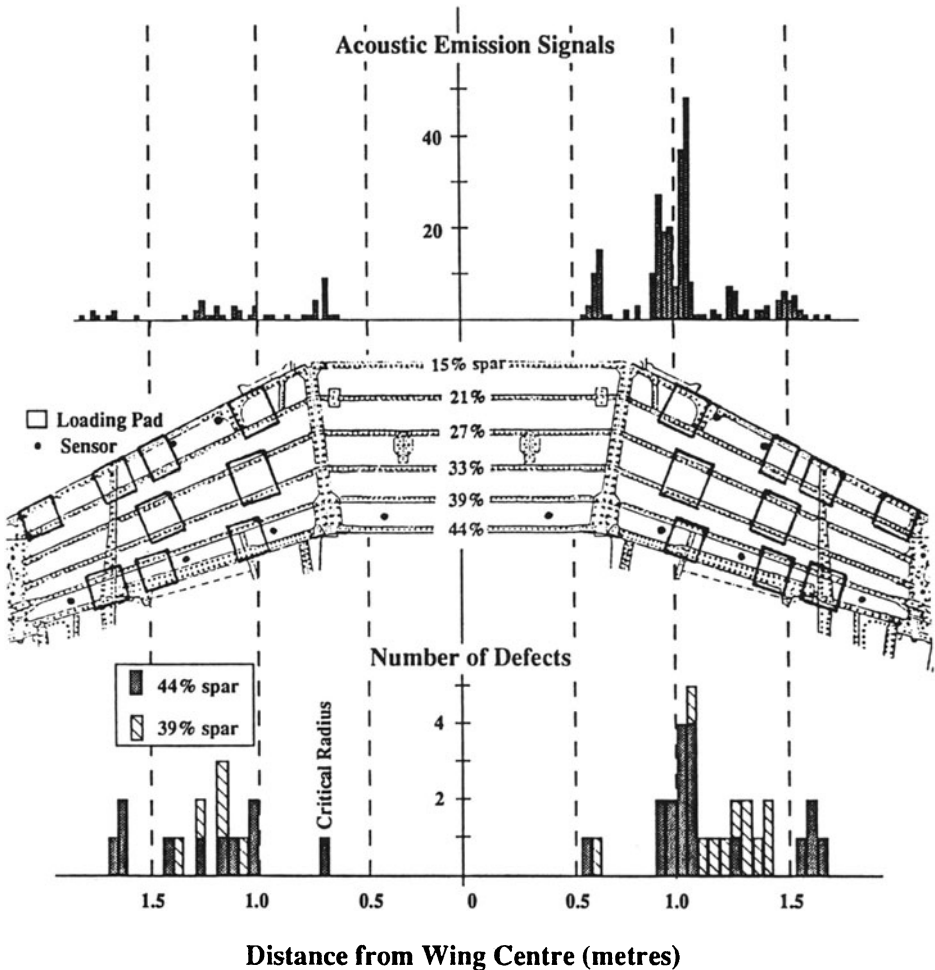

Fig. 4. Comparison of acoustic emission event histogram with the defect histogram. The acoustic emission data shows the number of events which occurred on the 39% and 44% spars during 68 maximum (100%) strain loadings (for strains greater than 95% of maximum). The defects are those measured inside fastener holes using eddy current inspection and confirmed by liquid penetrant inspection.

The acoustic emission data of Figure 4 predicts three areas of significant damage at 1m and 0.6m on the starboard side and at 0.7m on the port side. The severity of the crack related damage determines the number of detected events per 7g load cycle. For the region between 0.9m and 1.1m on the starboard side there is a total of 154 events in 50, 7g loading cycles indicating about 3 crack advances per 7g loading cycle. This could only result from fatigue crack growth at more than one source. The NDT results show six defects of varying size in this region. For the region between 0.55m and 0.7m there are 30 events, or about 1 event for every two 7g loading cycles indicating less crack advance. NDT revealed one defect in this location in the lower wing skin and continuing into the substructure. For the region 0.6m and 0.7m on the port side there were 17 events in 50, 7g loading cycles. NDT revealed a crack in the lower wing skin critical radius.

Also shown in Figure 4 is the histogram of all defects measured by eddy current inspection and confirmed by liquid penetrant inspection. Detection of the defects by the conventional NDT methods required removal of each fastener from the lower wing skin to permit access for the eddy current probe. The defects were found by progressive reaming of the fastener holes to range in depth from 0.3 to 1.2 mm. The agreement between the acoustic emission histogram and the defect histogram is striking and demonstrates clearly the applicability of acoustic emission to complex dispersive structures such as airframes. A comparison of the acoustic emission and defect histograms also leads us to the conclusion that all of the acoustic emission predictions of significant crack advance are in agreement with the identified defects; no significant defects were reported which were not predicted by acoustic emission.

It is interesting to note that the initial NDT inspection did not reveal the defects. This resulted from the fact that in the "unloaded" condition the cracks in the lower wing skin are in compression, a condition which is not uncommon for NDT inspection of aircraft fatigue-crack-prone areas. Further, confirmation of the defects in the 39% and 44% spars by NDT required the wing to be flexed by removing it from the fuselage, inverting it and applying loads at each end. If acoustic emission had not been used, irreparable damage would have occurred in the lower wing skin during subsequent dynamic loading.

CONCLUSIONS

A large area of the lower wing skin of a fighter aircraft was monitored during a ground durability and damage tolerance test. The presence of cracks in the lower wing skin and inner spar structure was predicted by acoustic emission. All acoustic emission predictions of crack locations were later confirmed using conventional NDT techniques (eddy current and LPI). No significant cracks were found by conventional NDT techniques which were not predicted by acoustic emission. NDT confirmation of some cracks predicted by acoustic emission required static loading of the structure to "open" the cracks. Further, had acoustic emission monitoring not been used, irreparable damage would have occurred in the lower wing skin during subsequent dynamic loading. This work clearly shows the superior sensitivity of acoustic emission compared to more conventional sensitive NDT techniques (eddy current, ultrasonics and liquid penetrant inspection) in this application. Acoustic emission also has the enormous advantage of providing very large area inspection of a complex bolted structure such as an aircraft wing or fuselage skin.

ACKNOWLEDGEMENTS

REFERENCES

1. T. F. Drouillard, <u>Acoustic Emission, A Bibliography with Abstracts</u> (Plenum Data Company, New York, 1979).
2. T. F. Drouillard, <u>Bibliography Update</u> (J. Acoust. Emis., 1982-90).
3. S. L. McBride and J. W. Maclachlan, J. Acoust. Emis., $\underline{1}$, 223-228 (1982).
4. S. L. McBride and J. W. Maclachlan, J. Acoust. Emis., $\underline{1}$, 229-235 (1982).
5. S. L. McBride and J. W. Maclachlan, J. Acoust. Emis., $\underline{3}$, 1-10 (1984).
6. S. L. McBride, M. D. Pollard, J. D. MacPhail, P. S. Bowman, and D. T. Peters, J. Acoust. Emis. $\underline{8}$, 4-7 (1989).